

This is the accepted manuscript made available via CHORUS. The article has been published as:

Electric-Field Control of Magnetization, Jahn-Teller Distortion, and Orbital Ordering in Ferroelectric Ferromagnets

Lan Chen, Changsong Xu, Hao Tian, Hongjun Xiang, Jorge Íñiguez, Yurong Yang, and L. Bellaiche

Phys. Rev. Lett. **122**, 247701 — Published 21 June 2019

DOI: [10.1103/PhysRevLett.122.247701](https://doi.org/10.1103/PhysRevLett.122.247701)

Electric-field control of magnetization, Jahn-Teller distortion and orbital ordering in ferroelectric ferromagnets

Lan Chen,^{1,2,3} Changsong Xu,¹ Hao Tian,^{2,3} Hongjun Xiang,^{4,5} Jorge Íñiguez,^{6,7} Yurong Yang,^{1,2,3,5,*} L. Bellaiche¹

¹*Physics Department and Institute for Nanoscience and Engineering,
University of Arkansas, Fayetteville, Arkansas 72701, USA*

²*National Laboratory of Solid State Microstructures,*

Department of Materials Science and Engineering, Nanjing University, Nanjing 210093, China

³*Jiangsu Key Laboratory of Artificial Functional Materials, Nanjing University, Nanjing 210093, China*

⁴*Key Laboratory of Computational Physical Sciences (Ministry of Education),*

State Key Laboratory of Surface Physics, and Department of Physics, Fudan University, Shanghai, 200433, China

⁵*Collaborative Innovation Center of Advanced Microstructures, Nanjing 210093, China*

⁶*Materials Research and Technology Department,*

Luxembourg Institute of Science and Technology,

5 avenue des Hauts-Fourneaux, L-4362 Esch/Alzette, Luxembourg

⁷*Physics and Materials Science Research Unit, University of Luxembourg, 41 Rue du Brill, L-4422 Belvaux, Luxembourg**

Controlling the direction of the magnetization by an electric field in multiferroics that are both ferroelectric and strongly ferromagnetic will open the doors to the design of next generation of spintronics and memory devices. Here, using first-principles simulations, we report the discovery that $\text{PbTiO}_3/\text{LaTiO}_3$ (PTO/LTO) superlattice possesses such highly-desired control, as evidenced by the electric-field-induced rotation of 90° and even full possible reversal of its magnetization in some cases. Moreover, such systems also exhibit Jahn-Teller distortions, as well as orbital orderings, that are switchable by electric field, therefore making PTO/LTO of importance for the tuning of electronic properties too. The origin for such striking electric-field controls of magnetization, Jahn-Teller deformations and orbital orderings resides in the existence of three different types of energetic coupling: one coupling polarization with anti-phase and in-phase oxygen octahedral tiltings; a second one coupling polarization with anti-phase oxygen octahedra tilting and Jahn-Teller distortions; and finally a biquadratic coupling between anti-phase oxygen octahedral tilting and magnetization.

Multiferroic materials hold promise for use in next-generation memory devices in which, e.g., electric field controls magnetism [1, 2]. Such materials are rare, owing to a typical incompatibility between ferroelectricity and magnetism [3]. This incompatibility has motivated an extensive search for new multiferroic materials [4–9], in which an electric-field control of magnetism was also investigated. For instance, the weak ferromagnetism and Dzyaloshinskii-Moriya (DM) vector in BiFeO_3 can be switched by 180° under electric field by a two-step sequential rotation of the polarization [10]. Moreover, the weak ferromagnetism of hybrid improper ferroelectrics superlattices, such as $\text{BiFeO}_3/\text{NdFeO}_3$ [11] and $\text{BiFeO}_3/\text{LaFeO}_3$ [12], and of Ruddlesden-Popper oxides with B-site cation ordered $\text{A}_3\text{BB}'\text{O}_7$ [13] was also predicted to be controllable by electric field, because the polarization is coupled with other non-polar lattice distortions. However, all these latter multiferroics possess a predominant antiferromagnetic alignment, that is, they “only” have a weak ferromagnetism and/or are ferrimagnetic [14, 15]. On the other hand, strong ferromagnetism has been found or predicted in EuTiO_3 [16], BiMnO_3 [17], $\text{La}_2\text{NiMnO}_6/\text{R}_2\text{NiMnO}_6$ [7] and $\text{A}^{2+}\text{TiO}_3/\text{R}^{3+}\text{TiO}_3$ [18] multiferroics, but electric-field control of such ferromagnetism has not been documented there. As a result, we are not aware that strong ferromagnetism has ever been reported to be controllable by electric field in any single phase of any multiferroics.

Moreover, Jahn-Teller distortion (JT) [19] and orbital order (OO) [20] are common phenomena in oxides, and are considered to be the origin of many physical behaviors. For instance, JT and OO effects are intimately linked to electronic properties, and lead to removing electronic degeneracy, opening band gaps and affecting magnetic properties. Furthermore, JT and OO effects play an important role in colossal magnetoresistance phenomena in manganites [21], superconductivity [22], polarization in perovskites [23, 24] and strong electronic correlation [25]. It is also highly desirable for functionality to tune JT distortions, OO and corresponding electronic properties by electric field. Note that Varignon *et al.* [24, 26] showed that JT can influence magnetic and orbital orderings, and suggested that magnitude of JT can be tuned by electric field in some perovskites, however, the switchability of JT and OO are unknown.

Here, by means of first-principle calculations, we investigate electrical, electronic and magnetic properties of $\text{PbTiO}_3/\text{LaTiO}_3$ (PTO/LTO) superlattices as well as their change under electric field. These simulations show that PTO/LTO superlattices are magnetoelectric ferroelectrics, as similar to Ref. [18], and possess a strong magnetization that can be switched by 90° under electric field being perpendicular to the initial polarization – consequently leading to a possible electric-field-induced reversal of ferromagnetism via a two-step process. This control of magnetization originates from a bi-quadratic

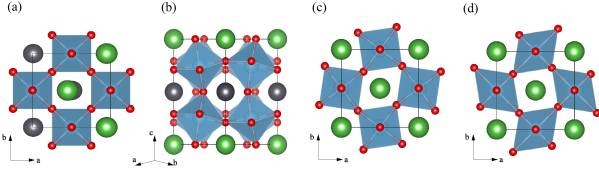


FIG. 1. (color online): Geometry and major structural distortions of the ground state of the studied PTO/LTO superlattice. (a) Polarization distortion P about the in-plane \mathbf{b} axis ($[-110]$ direction); (b) anti-phase oxygen octahedral rotations Φ_{xy} about the in-plane \mathbf{a} axis ($[110]$ direction); (c) in-phase oxygen octahedral rotations Θ_z about the out-of-plane \mathbf{c} axis ($[001]$ direction); and (d) Q Jahn-Teller lattice distortion..

energetic coupling between magnetization and anti-phase oxygen octahedral rotations, with these latter quantities being also coupled with polarization via trilinear couplings. We additionally found that electric field can also switch the JT and OO vectors when the electric field is antiparallel to the initial direction of the polarization. These new phenomena of control strong ferromagnetism, Jahn-Teller distortion and orbital ordering provide a new avenue to tune magnetic and electronic properties, in particular, and functionality, in general, in perovskites.

Structural, electronic and magnetic properties. Density-functional calculations were performed on PTO/LTO superlattices. Technically, $[\text{PTO}]_1/[\text{LTO}]_1$ superlattices are investigated here, for which one unit layer of PbTiO_3 successively alternates with one unit layer of LaTiO_3 along the pseudocubic $[001]$ direction. Structures, electric and magnetic properties without applying electric field and under electric field are investigated. More details about the method are given in the Supplemental Material [18, 27–35]. PbTiO_3 bulk possesses a tetragonal polar ground state (space group $P4mm$) with a polarization pointing along \mathbf{c} . On the other hand, the ground state of LaTiO_3 is an orthorhombic nonpolar phase (space group $Pbnm$) with an in-plane antiphase oxygen octahedral tilting and an out-of-plane in-phase oxygen octahedral tilting (which constitute antiferrodistortive (AFD) motions having the $a^-a^-c^+$ pattern in Glazer’s notations [36]). We numerically found that the PTO/LTO superlattice adopts a monoclinic phase (space group $P2_1$) with a similar $a^-a^-c^+$ AFD pattern as LTO. The lattice constants of this superlattice ($a=5.58$ Å, $b=5.63$ Å, and $c=7.91$ Å) are close to the average of the those of cubic PTO ($a_1\sqrt{2}=5.56$ Å, $a_2\sqrt{2}=5.56$ Å, and $2a_3=7.86$ Å) and LTO ($a=5.61$ Å, $b=5.71$ Å, and $c=7.87$ Å) bulks. Note that the predicted lattice constants of PTO and LTO agree rather well with experiments (the difference is less than 1.5%) [37, 38].

We further found that the charge order between Ti^{4+} in PTO and Ti^{3+} in LTO induces striking structural features and electronic properties in the PTO/LTO superlattice. More precisely, there are two Ti d^1 and two Ti

d^0 ions in our supercell, with these two types of Ti ions being arranged in a rocksalt configuration within the B-sublattice. In other words, the nearest neighbors of Ti d^1 ions in the B-sublattice are Ti d^0 ions, and *vice versa*. This d^1 - d^0 charge ordering generates a breathing distortion of oxygen octahedral cages (B_{OC}), for which the Ti^{3+} d^1 orbital occupation expands the corresponding oxygen octahedral cage while the Ti^{4+} d^0 orbital occupation shrinks the corresponding oxygen octahedral cage. Note that, in order to investigate the orbitals of Ti ions in details, we studied the projected density of states on Ti ions. We found that the Ti^{4+} ions have almost empty d orbital, while the Ti^{3+} ions display a mixed $d_{xy}+d_{xz}$ or $d_{xy}+d_{yz}$ character. These latter strong hybridizations of two d orbitals lead to an insulating character in the PTO/LTO system, as similar to the case of ferromagnetic $\text{A}^{2+}\text{TiO}_3/\text{R}^{3+}\text{TiO}_3$ superlattices ($\text{A}=\text{Sr}, \text{Ca}, \text{Ba}$; $\text{R}=\text{Sm}, \text{Y}, \text{Tm}, \text{La}, \text{Pr}, \text{Lu}$) [18], in which similar charge and orbital orderings are found. As a matter of fact, these hybridizations of two orbitals $d_{xy}+d_{xz}$ or $d_{xy}+d_{yz}$ result in the presently considered system being ferromagnetic semiconductor on the basis of intra-site Hund’s rules [18]. Practically, the computed band gap is 0.5 eV and the energy of the ferromagnetic configuration is lower than that of the A-type antiferromagnetic (A-AFM) configuration by 10 meV per Ti^{3+} ion. Moreover, from our non-collinear magnetic configuration calculations, the PTO/LTO system has mainly ferromagnetism lying along the in-plane \mathbf{b} direction with a magnetic moment of about $0.99 \mu_B$ per Ti^{3+} accompanied by a weak ferromagnetism being along the out-of-plane \mathbf{c} direction and of about $0.03 \mu_B$ magnitude per a supercell. The PTO/LTO superlattice has also a polarization oriented along the $-\mathbf{a}$ direction with a magnitude of $16.9 \mu\text{C}/\text{cm}^2$, which has the character of hybrid-improper ferroelectricity as discussed below [7, 39].

Moreover, the $P2_1$ ground state of PTO/LTO consists of a combination of several lattice distortions of the high-symmetry ($P4/mmm$) double perovskite. Such ground state possesses four main phonon modes having large magnitude: (1) a ferri-like polar A-cation motions [40], where Pb and La ions move in opposite direction and with different amplitude, which results in a polar mode (P), as depicted in Fig. 1a [11]; (2) an anti-phase tilting of oxygen octahedra about the \mathbf{a} -axis (Φ_{xy} , see Fig. 1b); (3) an in-phase tilting about the \mathbf{c} -axis (Θ_z , see Fig. 1c); and (4) the B_{OC} breathing motion that is related to the charge order between Ti^{4+} and Ti^{3+} ions and that expands or contracts oxygen octahedra. In the ground state of PTO/LTO superlattice, there is another mode, which is of Jahn-Teller nature (Q_z , see Fig. 1d) and which has an amplitude much smaller than the other four aforementioned modes, but the Jahn-Teller mode plays a key role in electronic properties and may couple to polarization and other distortion modes.

We then perform a free energy expansion in terms of

these lattice distortions and identify the following couplings [18, 26, 41–43]:

$$\mathcal{F} \propto P_x \Phi_x \Theta_z, P_y \Phi_y \Theta_z, P_x \Phi_x Q_z, P_y \Phi_y Q_z, \quad (1)$$

where the x , y and z subscripts refer to Cartesian components along the corresponding axis.

We project out the contribution of each Φ , Θ , Q and P modes to the $P2_1$ ground state structure and calculate the energy surface around the $P4/mmm$ reference structure by individually condensing each mode. Figure 2a displays the resulting total energy as a function of the amplitude of each distortion for these four modes. One can clearly see that the P mode, by itself, is stable, whereas large energy gains occur for Φ_{xy} and Θ_z – resulting in characteristic double-well potentials. Though the potential surface of Q_z is very flat with the magnitude of this mode, the inset of Fig. 2a indicates that the Q_z mode in $P4/mmm$ structure is barely unstable. The black squares (red circles, respectively) in Fig. 2b display the total energy of the state as a function of the amplitude of P , but with freezing Φ_{xy} and Θ_z (Φ_{xy} , Θ_z and Q_z , respectively) distortions to those of the ground state. In contrast to the single minimum of P at $P=0$ in Fig. 2a when the other modes are null, polarization in Fig. 2b becomes unstable and its minimum shifts to a nonzero value. The resulting energy gain when freezing Φ_{xy} , Θ_z and Q_z is more than that obtained when only freezing Φ_{xy} and Θ_z . The energy as a function of amplitude of P when freezing Φ_{xy} and Q_z (not shown here) also exhibits a single well, similar to that shown in Fig. 2b but with smaller energy gain. These features are direct indications that both trilinear couplings $P\Phi\Theta$ and $P\Phi Q$ of Eq. 1 are in play here. These trilinear couplings lead to a polarization of $16.9 \mu\text{C}/\text{cm}^2$.

Properties under electric field. These observations of two types of trilinear couplings between P , Φ , Θ and Q also suggest that the switching of polarization by electric field may induce the switching of Φ , or the switching

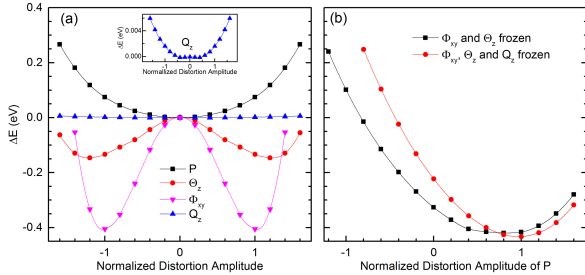


FIG. 2. (color online): Dependence on the total energy on amplitude of distortion in the investigated PTO/LTO superlattice. (a) Energy with respect to the amplitude of the main four lattice distortions, P , Φ_{xy} , Θ_z and Q_z . (b) Energies as a function of amplitude of P when fixing Φ_{xy} and Θ_z (black squares), as well as that when fixing Φ_{xy} , Θ_z and Q_z (red circles), to their values in the ground state.

of both Θ and Q . We first consider the case of switching the polarization by 90° , by applying an electric field along $-\mathbf{b}$, that is perpendicular to the initial polarization lying along $-\mathbf{a}$. Figure 3a represents the energy difference ($\Delta E_{FM_a-FM_b}$) between the ferromagnetic spin configurations along \mathbf{a} and \mathbf{b} , as well as the polarization (P) and AFD angles (Φ, Θ) as a function of this applied electric field. Under electric field ranging from 0 to 0.062 V/\AA , the \mathbf{a} -component of the polarization keeps a value of about $-16 \mu\text{C}/\text{cm}^2$, while its \mathbf{b} -component increases in magnitude from about zero to $-33 \mu\text{C}/\text{cm}^2$. Under this electric field range of $0 - 0.062 \text{ V/\AA}$, the AFD (antiphase) angles Φ_x and Φ_y both keep a value of about 7° and the AFD (in-phase) Θ_z remains to be about -7.4° . The magnetic easy axis is along \mathbf{b} or $-\mathbf{b}$ (these two opposite directions are symmetrically equivalent), as indicated by the energy difference shown in top panel of Fig. 3a. At the electric field of 0.063 V/\AA , the polarization P , the in-plane anti-phase oxygen octahedra tilting Φ , and the magnetic easy axis are all switched by 90° with respect to the case under no field. More precisely, polarization is switched to $-\mathbf{b}$, Φ_x is reversed from 7° to -7° (resulting in the axis of rotation of the antiphase tilting switching from \mathbf{a} to \mathbf{b}) and the magnetic easy axis is now aligned along \mathbf{a} . When the electric field along \mathbf{b} further increases to 0.085 V/\AA , the polarization further increases in magnitude from $71 \mu\text{C}/\text{cm}^2$ to $79 \mu\text{C}/\text{cm}^2$, while the x , y and z components of the AFD tilting are now about -6.5° , 6.2° , and -7° respectively. Meanwhile, the $\Delta E_{FM_a-FM_b}$ energy difference between the magnetic easy axes \mathbf{a} and \mathbf{b} is always negative and its magnitude slightly increases when electric field further increases, therefore stabilizing even more an easy magnetic axis along \mathbf{a} .

Furthermore, when the electric field is released (see black open symbols in Fig. 3a), P , Φ_y , Θ and $\Delta E_{FM_a-FM_b}$ do not change their sign. In other words, after removal of a large enough electric field, P , Φ , and the magnetic easy axis all undergo a switching by 90° with respect to the initial zero-field state. These promising switching of strong ferromagnetism shown in Fig. 3a have never been found in any material. [10–13, 44].

It is known, from the knowledge of magnetic space group and group theory [12], that anti-phase oxygen octahedral rotation controls the orientation of the magnetization. To better understand the mechanism of the aforementioned switching of strong ferromagnetism, we also determined couplings between AFD and magnetism order parameters, which are found to be of the form:

$$\mathcal{F} \propto \Phi_x \Phi_y M_x M_y \quad (2)$$

where Φ_x , Φ_y are anti-phase oxygen octahedra tiltings along the pseudocubic $[100]$ and $[010]$ directions respectively, while M_x and M_y are the components of the magnetization along the $[100]$ and $[010]$ directions, respectively. The ground state of Fig. 3a under zero electric field possesses a magnetic moment given by $M_x = -1.41 \mu_B$

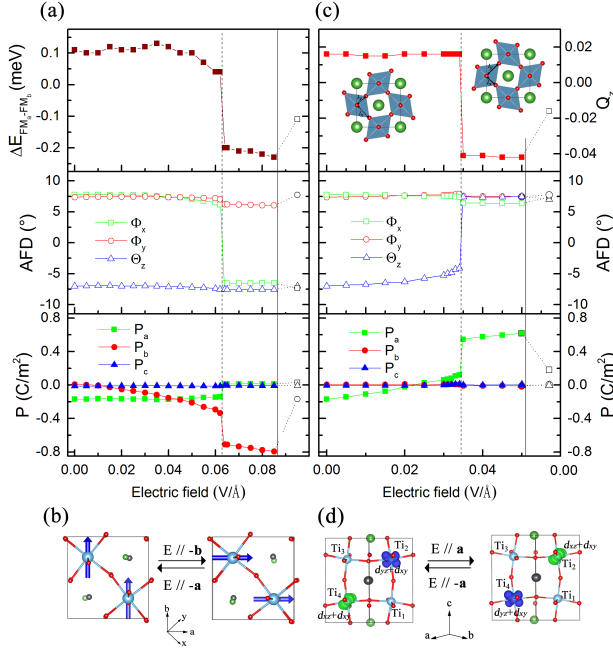


FIG. 3. (color online): Physical quantities as a function of electric field (panels a and b) applied along $-\mathbf{b}$, i.e., perpendicular to the initial direction of the polarization, and (panels c and d) applied along \mathbf{a} , i.e., antiparallel to the initial direction of the polarization, in the studied PTO/LTO superlattice. (Panel a): Energy difference between ferromagnetic configurations along \mathbf{a} and \mathbf{b} ; oxygen octahedral tilting angles, Φ_x , Φ_y and Θ_z ; and polarization \mathbf{P} ; (Panel b): Schematization of the spin configurations on Ti^{3+} ions, that can be switched by 90° via the application of electric fields oriented along the $-\mathbf{b}$ axis or the $-\mathbf{a}$ axis. (Panel c): JT distortion Q_z ; oxygen octahedral tilting angles and polarization. (Panel d): Charge density of states near the Fermi level in energy range from -0.5 eV to 0 eV. The black open symbols in Panels (a) and (c) represent the same quantities when the electric field is released.

and $M_y = 1.41 \mu_B$ per 20 atoms (which is therefore mostly along the \mathbf{b} orthorhombic axis), and an anti-phase tilting quantified by $\Phi_x = 7^\circ$ and $\Phi_y = 7^\circ$. We found that this phase transforms, under the application of an aforementioned large enough electric field applied along $-\mathbf{b}$, followed by a removal of such field, to another energetically degenerate phase having a magnetic moment given by $M_x = M_y = 1.41 \mu_B$ (which is mostly along \mathbf{a}), and an anti-phase tilting given by $\Phi_x = -7^\circ$ and $\Phi_y = 7^\circ$. According to Eq. (2), such change of sign of M_x originates from the electric-field-induced reversal of Φ_x .

We thus found that a large enough electric field applied perpendicularly to the initial direction of the polarization can transform PTO/LTO from adopting a Phase I $[\mathbf{M}_b, \Phi_a, \mathbf{P}_{-a}]$ to another Phase II $[\mathbf{M}_a, \Phi_b, \mathbf{P}_{-b}]$. As schematized in Figs. 3b, applying an electric field along $-\mathbf{a}$ to this Phase II should then either make the system come back to its initial Phase I $[\mathbf{M}_b, \Phi_a, \mathbf{P}_{-a}]$ or to another

phase with $[\mathbf{M}_{-b}, \Phi_a, \mathbf{P}_{-a}]$, since changing the magnetization from \mathbf{M}_b to \mathbf{M}_{-b} has no effect on the bi-quadratic energy of Eq. (2). Moreover, following Eqs. (1) and (2) also implies that applying now an electric field along \mathbf{a} to this Phase II $[\mathbf{M}_a, \Phi_b, \mathbf{P}_{-b}]$ should then transform it into a Phase III characterized by $[\mathbf{M}_{-b}, \Phi_{-a}, \mathbf{P}_a]$ or into a Phase IV for which $[\mathbf{M}_b, \Phi_{-a}, \mathbf{P}_a]$. As a result, this two-step process opens the door to reversing a strong ferromagnetic moment by application of electric fields, which is a possibility unheard of. Yet, from our calculations, we can only say that the switch only has a 50% chance to occur.

We next consider the situation of applying electric fields to Phase I along the opposite direction of its polarization (that is, we apply an electric field along $+\mathbf{a}$). Under such electric fields with a magnitude ranging from zero to 0.034 V/\AA and as shown in Fig. 3c, the polarization smoothly changes its \mathbf{a} -component from (negative) $-17 \mu\text{C}/\text{cm}^2$ to (positive) $+12 \mu\text{C}/\text{cm}^2$ while the anti-phase in-plane tilting Φ_x and Φ_y keep almost the same value of 7.5° and the out-of-plane in-phase tilting reduces its value from -7° to -4.1° . To better describe the Jahn-Teller distortion of oxygen octahedra, we define its Q_z order parameter as the length difference between the Ti-O bond along the \mathbf{x} axis (called l_x in inset of Fig. 3c) and the Ti-O bond along the \mathbf{y} axis (denoted as l_y in inset of Fig. 3c and belonging to the same oxygen octahedron as l_x). Negative Q_z corresponds to shrinking in the \mathbf{x} direction and expansion in the \mathbf{y} direction while positive Q_z implies expansion along \mathbf{x} and shrinking along \mathbf{y} . From Fig. 3c, one can see that oxygen octahedra slightly expand in the \mathbf{x} direction under such electric field varying from zero to 0.034 V/\AA . At a field of 0.035 V/\AA , the polarization suddenly jumps from $12 \mu\text{C}/\text{cm}^2$ to $54 \mu\text{C}/\text{cm}^2$, the oxygen octahedral in-phase tilting Θ_z switches from -4.1° to $+6.4^\circ$, and Q_z changes from about 0.02 \AA to -0.04 \AA . The polarization P , in-phase tilting Θ and JT distortion Q_z therefore all revert their direction with respect to the case of null field. Under larger electric field, P , Φ , Θ and JT distortion nearly retain their values associated with the 0.035 V/\AA field. We also found that, when removing these large fields (see Fig. 3c), P , Θ and JT distortion Q do not change of direction (while their magnitude can be modified). In other words, JT patterns can be reverted by applying and then removing large enough electric field in PTO/LTO superlattice (Inset of Fig. 3c schematizes the two JT distortion patterns that are switchable by such electric fields) [19, 45].

Furthermore, Fig. 3d depicts the corresponding charge density of orbitals in the two phases which are switchable by electric field parallel (or antiparallel) to \mathbf{a} . The four Ti ions of our supercell are denoted by Ti_1 , Ti_2 , Ti_3 , and Ti_4 . Ti_1 and Ti_3 are $+4$ ions with essentially empty d shells, while Ti_2 and Ti_4 are $+3$ ions with one electron in d shell (also see Fig. S3 in Supplementary Materials). In the left panel of Fig. 3d (which corresponds to the initial zero-field ground state), the main orbitals on Ti_2

are $d_{yz} + d_{xy}$ versus $d_{xz} + d_{xy}$ for Ti_4 . When the JT distortion is reverted and as displayed in Fig. 3d, the main orbitals are now $d_{xz} + d_{xy}$ on Ti_2 , and $d_{yz} + d_{xy}$ on Ti_4 . The d_{yz} and d_{xz} orbitals are therefore switched between Ti_2 and Ti_4 under such electric field. A change of Jahn-Teller distortion patterns (see inset of Fig. 3c) leads to a specific change of the corresponding orbitals ($d_{xz} + d_{xy}$ versus $d_{yz} + d_{xy}$ for that specific Ti^{3+} ion). Consequently, switching the Jahn-Teller pattern by an electric field (as a result of a trilinear coupling indicated in Eq. (1)) subsequently results in the switching of orbital ordering. Such orbital effect may provide us a new way to modulate electronic structure and thus affect magnetism, superconductivity, topological properties, etc. [24, 26].

In summary, we demonstrated electronic control of strong ferromagnetism, JT distortion, and orbital ordering in the multiferroic PTO/LTO superlattice. Interestingly, the lattice parameters of PTO/LTO ($a=5.58$ Å, $b=5.63$ Å) are close (namely, less than 1%) to those of commercial substrates such as DyScO_3 , TbScO_3 , GdScO_3 , SmScO_3 , NdScO_3 and PrScO_3 . Growing epitaxial PTO/LTO films on these substrates, via, e.g., pulsed laser deposition and molecular beam epitaxy techniques, should thus be practically achievable. Note also that $\text{A}^{2+}\text{TiO}_3/\text{R}^{3+}\text{TiO}_3$ superlattices ($\text{A}=\text{Sr}, \text{Ca}, \text{Ba}$; $\text{R}=\text{Sm}, \text{Y}, \text{Tm}, \text{La}, \text{Pr}, \text{Lu}$) have similar ferroelectric and ferromagnetic properties than our PTO/LTO studied system [18]. We thus expect that the presently determined electrically induced switching of ferromagnetism, JT distortions and orbital ordering should also be realizable in $\text{A}^{2+}\text{TiO}_3/\text{R}^{3+}\text{TiO}_3$ superlattices.

Y.Y. and L.B. thank ONR Grant N00014-17-1-2818. C.X. acknowledges DOE, Office of Basic Energy Sciences, under Award # DE-SC0002220. L.B. and J.I. also thank the Luxembourg National Research Fund through Grant INTER/MOBILITY/15/9890527 (GREENOX). L.C, H.T and Y.Y. also acknowledge the state key program for basic research of China (Contract No.: 2015CB921203) and NSFC (Contract No.: 11874207).

* yangyr@nju.edu.cn

- [1] N. A. Spaldin and M. Fiebig, *Science* **309**, 391 (2005).
- [2] W. Eerenstein, N. Mathur, and J. F. Scott, *Nature* **442**, 759 (2006).
- [3] N. A. Hill, *J. Phys. Chem. B* **104**, 6694 (2000).
- [4] T. Kimura, T. Goto, H. Shintani, K. Ishizaka, T.-h. Arima, and Y. Tokura, *Nature* **426**, 55 (2003).
- [5] J. Wang, J. Neaton, H. Zheng, V. Nagarajan, S. Ogale, B. Liu, D. Viehland, V. Vaithyanathan, D. Schlom, U. Waghmare, *et al.*, *Science* **299**, 1719 (2003).
- [6] A. Kumar, R. Katiyar, R. N. Premnath, C. Rinaldi, and J. Scott, *J. Mater. Sci.* **44**, 5113 (2009).
- [7] H. J. Zhao, W. Ren, Y. Yang, J. Íñiguez, X. M. Chen, and L. Bellaiche, *Nat. Commun.* **5**, 4021 (2014).
- [8] M. J. Pitcher, P. Mandal, M. S. Dyer, J. Alaria, P. Borisov, H. Niu, J. B. Claridge, and M. J. Rosseinsky, *Science* **347**, 420 (2015).
- [9] M. Kenzelmann, A. B. Harris, S. Jonas, C. Broholm, J. Schefer, S. B. Kim, C. L. Zhang, S.-W. Cheong, O. P. Vajk, and J. W. Lynn, *Phys. Rev. Lett.* **95**, 087206 (2005).
- [10] J. Heron, J. Bosse, Q. He, Y. Gao, M. Trassin, L. Ye, J. Clarkson, C. Wang, J. Liu, S. Salahuddin, *et al.*, *Nature* **516**, 370 (2014).
- [11] B. Xu, D. Wang, H. J. Zhao, J. Íñiguez, X. M. Chen, and L. Bellaiche, *Adv. Func. Mater.* **25**, 3626 (2015).
- [12] Z. Zanolli, J. C. Wojdeł, J. Íñiguez, and P. Ghosez, *Phys. Rev. B* **88**, 060102 (2013).
- [13] X.-Z. Lu and J. M. Rondinelli, *Adv. Func. Mater.* **27**, 1604312 (2017).
- [14] H. Das, A. L. Wysocki, Y. Geng, W. Wu, and C. J. Fennie, *Nat. Commun.* **5**, 2998 (2014).
- [15] J. A. Mundy, C. M. Brooks, M. E. Holtz, J. A. Moyer, H. Das, A. F. Rébola, J. T. Heron, J. D. Clarkson, S. M. Disseler, Z. Liu, *et al.*, *Nature* **537**, 523 (2016).
- [16] J. H. Lee, L. Fang, E. Vlahos, X. Ke, Y. W. Jung, L. F. Kourkoutis, J.-W. Kim, P. J. Ryan, T. Heeg, M. Roederer, *et al.*, *Nature* **466**, 954 (2010).
- [17] M. Gajek, M. Bibes, A. Barthélémy, K. Bouzehouane, S. Fusil, M. Varela, J. Fontcuberta, and A. Fert, *Phys. Rev. B* **72**, 020406 (2005).
- [18] N. Bristowe, J. Varignon, D. Fontaine, E. Bousquet, and P. Ghosez, *Nat. Commun.* **6**, 6677 (2015).
- [19] J. B. Goodenough, *Annu. Rev. Mater. Sci.* **28**, 1 (1998).
- [20] A. I. Liechtenstein, V. I. Anisimov, and J. Zaanen, *Phys. Rev. B* **52**, R5467 (1995).
- [21] B. Raveau, M. Hervieu, A. Maignan, and C. Martin, *J. Mater. Chem.* **11**, 29 (2001).
- [22] J. G. Bednorz and K. A. Müller, *Rev. Mod. Phys.* **60**, 585 (1988).
- [23] C. Xu, Y. Li, B. Xu, J. Íñiguez, W. Duan, and L. Bellaiche, *Adv. Func. Mater.* **27**, 1604513 (2017).
- [24] J. Varignon, N. C. Bristowe, and P. Ghosez, *Phys. Rev. Lett.* **116**, 057602 (2016).
- [25] R. Berthelot, D. Carlier, and C. Delmas, *Nat. Mater.* **10**, 74 (2011).
- [26] J. Varignon, N. C. Bristowe, E. Bousquet, and P. Ghosez, *Scientific reports* **5**, 15364 (2015).
- [27] J. P. Perdew, A. Ruzsinszky, G. I. Csonka, O. A. Vydrov, G. E. Scuseria, L. A. Constantin, X. Zhou, and K. Burke, *Phys. Rev. Lett.* **100**, 136406 (2008).
- [28] G. Kresse and D. Joubert, *Phys. Rev. B* **59**, 1758 (1999).
- [29] J. Heyd, G. E. Scuseria, and M. Ernzerhof, *J. Chem. Phys.* **118**, 8207 (2003).
- [30] R. D. King-Smith and D. Vanderbilt, *Phys. Rev. B* **47**, 1651 (1993).
- [31] H. Fu and L. Bellaiche, *Phys. Rev. Lett.* **91**, 057601 (2003).
- [32] L. Chen, Y. Yang, and X. Meng, *Sci. Rep.* **6**, 25346 (2016).
- [33] B. Xu, J. Íñiguez, and L. Bellaiche, *Nat. Commun.* **8**, 15682 (2017).
- [34] Z. Jiang, Y. Nahas, S. Prokhorenko, S. Prosandeev, D. Wang, J. Íñiguez, and L. Bellaiche, *Phys. Rev. B* **97**, 104110 (2018).

- [35] P. Chen, R. J. Sichel-Tissot, J. Young Jo, R. T. Smith, S.-H. Baek, W. Saenrang, C.-B. Eom, O. Sakata, E. M. Dufresne, and P. G. Evans, *Appl. Phys. Lett.* **100**, 062906 (2012).
- [36] A. Glazer, *Acta Crystallogr. B Struct. Cryst. Cryst. Chem.* **28**, 3384 (1972).
- [37] O. Yamaguchi, A. Narai, T. Komatsu, and K. Shimizu, *J. Am. Ceram. Soc.* **69**, C (1986).
- [38] M. Eitel and J. Greedan, *J. Less. Common. Met.* **116**, 95 (1986).
- [39] N. A. Benedek and C. J. Fennie, *Phys. Rev. Lett.* **106**, 107204 (2011).
- [40] A. T. Mulder, N. A. Benedek, J. M. Rondinelli, and C. J. Fennie, *Adv. Func. Mater.* **23**, 4810 (2013).
- [41] T. Fukushima, A. Stroppa, S. Picozzi, and J. M. Perez-Mato, *Physical Chemistry Chemical Physics* **13**, 12186 (2011).
- [42] J. M. Rondinelli and C. J. Fennie, *Advanced Materials* **24**, 1961 (2012).
- [43] N. Miao, N. C. Bristowe, B. Xu, M. J. Verstraete, and P. Ghosez, *Journal of Physics: Condensed Matter* **26**, 035401 (2013).
- [44] P. S. Wang, W. Ren, L. Bellaiche, and H. J. Xiang, *Phys. Rev. Lett.* **114**, 147204 (2015).
- [45] H. Köppel, D. R. Yarkony, and H. Barentzen, *The Jahn-Teller Effect* (Springer, New York, 2007).